

Low-temperature Liquid Exfoliation of Milligram-scale Single Crystalline Few-layer β 12-Borophene Sheets as Efficient Electrocatalysts for Lithium–Sulfur Batteries

Haojian Lin

Sun Yat-sen University

Haodong Shi

Dalian Institute of Chemical Physics, Chinese Academy of Sciences

Zhen Wang

Dalian Institute of Chemical Physics

Yue-Wen Mu

Shanxi University <https://orcid.org/0000-0002-0162-5091>

Si-Dian Li

Shanxi University <https://orcid.org/0000-0001-5666-0591>

Jijun Zhao

Dalian University of Technology

Jingwei Guo

Dalian Institute of Chemical Physics

Bing Yang (✉ byang@dicp.ac.cn)

Dalian Institute of Chemical Physics <https://orcid.org/0000-0003-3515-0642>

Zhong-Shuai Wu

Dalian Institute of Chemical Physics, Chinese Academy of Sciences <https://orcid.org/0000-0003-1851-4803>

Fei Liu

Sun Yat-sen University <https://orcid.org/0000-0001-7603-9436>

Article

Keywords: Two-dimensional (2D) borophene, lithium sulfur (Li-S) batteries, low-temperature liquid exfoliation (LTLE) method

Posted Date: February 24th, 2021

DOI: <https://doi.org/10.21203/rs.3.rs-209092/v1>

License:  This work is licensed under a Creative Commons Attribution 4.0 International License.

[Read Full License](#)

Abstract

Two-dimensional (2D) borophene is predicted as an ideal electrode material for lithium sulfur (Li-S) batteries because of low-density, metallic conductivity, high Li-ion surface mobility and strong interface bonding energy to polysulfide. But until now, 2D borophene-based Li-S batteries have not yet been achieved due to the absence of massive synthesis method. Herein, we developed a novel low-temperature liquid exfoliation (LTLE) method for scalable synthesis of single crystalline 2D few-layer β_{12} -borophene sheets with a C_{2v} symmetry. The as-synthesized 2D sheets were used as the polysulfide immobilizers and electrocatalysts of Li-S batteries for the first time. The resulting Li-S cells employing borophene sheets delivered a strikingly high areal capacity of 5.2 mAh cm^{-2} at a high sulfur loading of 7.8 mg cm^{-2} with an ultralow capacity fading rate (0.039 % per cycle) in 1000 cycles, outperforming most of the Li-S batteries employing other 2D materials. Under the help of few-layer β_{12} -borophene, their high-activity behaviors should be attributed to the significant enhancement of both the Li-ion's surface migration and the adsorption energy for Li_2S_n clusters based on density functional theory (DFT) models. Our research reveals great potential of 2D β_{12} -borophene sheets in future high-performance Li-S batteries.

Introduction

The rapid development of electrochemical energy storage devices in the fields of electric vehicles, portable electronic devices and large-scale smart power grids continuously drive the researchers to explore lower cost, higher energy density, and better safety batteries than current lithium-ion batteries¹⁻⁴. Among many candidates, lithium sulfur (Li-S) batteries have been gaining the global attention due to their overwhelming energy density (2600 Wh kg^{-1}), natural abundance and environment-friendly of sulfur feedstock⁵⁻⁹. However, the existence of internal polysulfide shuttling, large volume expansion of sulfur and sluggish redox kinetics inevitably lead to the sharp deterioration of the electrochemical performances of Li-S batteries¹⁰⁻¹².

Considering the irreversible loss and inefficient utilization of sulfur cathodes, much effort has been devoted to the design of advanced materials for immobilizing and activating sulfur materials, such as transitional-metal oxides^{13,14}, sulfides¹⁵⁻¹⁷, carbides,¹⁸⁻²⁰ metal nitrides²¹⁻²³ and heterostructures²⁴⁻²⁶. Recently, two-dimensional (2D) materials with strong in-plane covalent bonds and weak interlayered van der Waals (vdW) forces have been intensively studied because of their superior advantages over traditional bulk materials for Li-S cell applications^{27,28}. 2D materials such as siloxane²⁹, black phosphorene^{30,31}, BN^{32,33}, C_3N_4 ^{34,35}, and MXene^{36,37}, were found to exhibit excellent catalytic activities towards polysulfides because of their extraordinary surface properties. However, most of these 2D material-based Li-S cells still have some disadvantages, such as low capacity³⁸, slow charge-discharge rate^{39,40}, structure instability^{38,41}, and poor cyclic stability³². Hence, the design and development of novel 2D materials are highly demanded towards high-performance Li-S batteries with large catalytic activity, high-efficient adsorption, fast conversion of polysulfides and long-term durability.

As a typical 2D Dirac material consisted of the lightest solid element, 2D borophene with unique surface configuration and complex multicenter-two electron bonds has been earlier predicted as an ideal electrode material for Li-S batteries due to its native metallic conductivity⁴², large elastic modulus⁴³, heavy anisotropy⁴⁴, high Fermi velocity (6.6×10^5 m/s)⁴⁵, excellent thermal and chemical stability⁴⁶, large Li-ion surface mobility as well as strong bonding energy to polysulfide clusters⁴⁷. However, borophene-based Li-S cells have not yet been achieved for practical use so far owing to the absence of a facile route for the scalable production of 2D borophene nanomaterials.

In this work, we developed a low-temperature liquid exfoliation (LTLE) strategy for scalable production of single crystalline borophene sheets as efficient polysulfide electrocatalyst for Li-S batteries. Few-layer 2D borophene sheets with β_{12} -phase were thus identified with an average flake size of ~ 3 μm and an ultrathin thickness less than 10 atomic layers. The β_{12} -borophene sheets exhibited extraordinary performances as efficient immobilizer and electrocatalyst for advanced Li-S batteries, showing excellent rate performance of 721 mAh g^{-1} at 8 C ($1 \text{ C} = 1675 \text{ mAh g}^{-1}$) and an ultralow decay rate of less than 0.039 % in 1000 continuous cycling measurements. More impressively, the areal capacity can arrive as high as 5.2 mAh cm^{-2} at a large sulfur loading of 7.8 mg cm^{-1} in lean electrolyte with a ratio of electrolyte to sulfur (E/S) ratio of 6.8 ml g^{-1} . Our work suggests that single crystalline few-layer borophene sheets hold great potential for high-efficiency Li-S batteries.

Results And Discussions

The LTLE synthesis process of few-layer borophene sheets is schematically illustrated in Fig. 1a. By optimizing the sonication power and solvent concentration, massive production of 2D borophene sheets has been successfully achieved. N-methyl pyrrolidone (NMP) was found to be the most effective among a series of solvents adopted in our experiment, as seen in Supplementary Figs. 1 and 2. The color of the product solution is dark-brown or dark-black in Fig. 1b, varying with the sheet concentration. Moreover, the mass of 2D sheets reaches as high as 10 mg and their yield is over 20 %, evidently increased compared with previous reports (≤ 10 %^{48,49}). The low-temperature approach is thus believed to improve the exfoliation efficiency of non-layered bulk materials, because of which significantly enhances the anisotropy discrepancy between the in-plane and out-of-plane covalence bonds⁵⁰. Scanning electron microscope (SEM) and atomic force microscope (AFM) images of the as-grown products are respectively in Fig. 1c, d, where ultrathin 2D borophene sheets are observed to have an edge length of $2 \sim 5$ μm and exhibit uniform and smooth appearance. The thickness of 2D sheet is observed to be only $1.32 \sim 2.32$ nm, suggesting its ultra-thin nature.

X-ray diffraction (XRD) pattern of 2D borophene sheets (Supplementary Fig. 3) shows the same characteristic diffraction pattern as that of the theoretically calculated β_{12} -borophene using density functional theory (DFT), clearly different from that of the bulk β -rhombohedral boron powder (JCPDS No. 00-031-0207). As seen in Fig. 1e, the X-ray photoelectron spectrum (XPS) of B 1s core level is consisted of two characteristic components, attributed to the B-B species at 187.5 eV ⁵¹ and the B-O species at 189.1

eV⁵², respectively. And the molar ratio of the B-B to B-O species is estimated to be more than 94 %, suggesting a majority of pure boron composition in 2D borophene sheets. The minor B-O species are supposed to originate from the edge oxidation of borophene sheets during the short exposure to the air after being taken out for XPS measurements (Supplementary Fig. 4)⁵².

Raman spectroscopy was employed to better differentiate the 2D borophene sheets from the bulk boron powders^{53,54}. Four Raman peaks of 2D borophene sheets are clearly identified (Fig. 1f) as the fingerprints of β_{12} phase⁵⁵, differing from those of bulk boron with β -rhombohedral phase. Accordingly, the strong peak at $\sim 268 \text{ cm}^{-1}$ is ascribed to the out-of-plane bending vibration mode of β_{12} phase⁵⁵. And the other peaks at ~ 423 , ~ 901 and $\sim 1017 \text{ cm}^{-1}$ are respectively indexed as the , and modes, resulting from the in-plane stretching modes of β_{12} phase⁵⁵.

Transmission electron microscopy (TEM) was performed to determine the surface configuration of 2D borophene sheets. A typical TEM image in Fig. 2a exhibits a similar planar morphology in line with the aforementioned SEM and AFM results (Fig. 1c, d). Close examination (Fig. 2a inset) reveals an ultrathin thickness of only 6 atomic layers with an adjacent planar distance of 5.1 Å. The high-resolution TEM (HRTEM) image further verifies high-quality single crystal nature of 2D borophene sheets. As shown in Fig. 2b, the 2D borophene sheets are found to have a hexagonal honeycomb lattice with a perfect planar periodicity of $a = b \approx 2.76 \text{ Å}$ and the intersection angle θ of about 120° in the unit cell. Based on the DFT calculations, we thus propose a novel allotrope with symmetry (referred to as β_{12} -B₅) for few-layer β_{12} -borophene sheets, where there are 5 boron atoms in a unit cell (Fig. 2c). In this model, both of the lattice constants (a and b) of few-layer borophene are 2.83 Å and the angle θ between a and b vectors is equal to 120° , which are in good agreement with the HRTEM results (Fig. 2b). Based on the theoretical model, the bright contrasts in the HRTEM image (Fig. 2b) thus correspond to the six-member rings of the boron honeycomb lattice (Fig. 2c). Besides, the layer distance of adjacent (001) planes is theoretically calculated to be about 5.0 Å for β_{12} -B₅ borophene, nearly identical to the experimental results (5.1 Å) measured by TEM. Statistically, the thickness of most of the 2D sheets is less than 5 nm. (Supplementary Fig. 5a). Therefore, the atomic layer numbers of the as-synthesized borophene sheets should be less than 10, unveiling the ultrathin nature of few-layer borophene. In addition, the 2D β_{12} -borophene sheets are thermodynamically stable as evidenced by the absence of any negative frequency in the entire Brillouin zone (Fig. 2d) according to the density functional perturbation theory (DFPT). Similar calculations are carried out on the (104) plane (Supplementary Fig. 5), which are also in good agreement with our experimental results. High-angle annular dark-field scanning transmission electron microscope (HAADF-STEM) and energy dispersive X-ray spectroscopy (EDX) mapping (Fig. 2e-h) images also reveal a uniform distribution of boron element across the 2D sheet with a pure boron content over 98 %, which is in good consistent with the electron energy loss spectrum (EELS) (Supplementary Fig. 5b).

Based on all characterizations mentioned above, we can thus conclude that single crystalline few-layer borophene sheets with β_{12} -B₅ phase were successfully synthesized using LTLE. In comparison with other

synthetic methods summarized in Supplementary Table 1, our route is thus low-cost, facile and high-efficient for scalable production of single crystalline β_{12} -borophene sheets towards practical applications such as Li-S battery.

To demonstrate the catalytic activity of few-layer β_{12} -borophene sheets for Li-S battery, the potentiostatic experiments were carried out to monitor the liquid-solid conversion in the nucleation and growth of Li_2S from polysulfides. The galvanostatic discharge was respectively performed on CNT/ β_{12} -borophene (CNT/B) and bare CNT hosts at 2.05 V, in which 0.01 V overpotential was used to induce the generation of Li_2S . All the cells reached the highest potentiostatic current after about 1000 s, but the nucleation abilities of Li_2S were found to be completely different, causing a capacity of 193 mAh g^{-1} and 72 mAh g^{-1} for CNT/B and CNT electrodes, respectively (Fig. 3a). Besides, the dissolution ability of solid Li_2S was also remarkably promoted by the implantation of few-layer β_{12} -borophene. After the fully conversion of sulfurs into Li_2S , the Li_2S dissolution was kinetically evaluated by using a potentiostatic charge process. Clearly, a larger oxidation current was detected on CNT/B (0.13 mA cm^{-2}) enabled cell in comparison with bare CNT electrode (0.11 mA cm^{-2}), unveiling the excellent electrocatalysis behaviors of 2D β_{12} -borophene in enhancing the dissolution of Li_2S (Fig. 3b).

To gain insight into the enhancement effect of β_{12} -borophene sheets on the liquid-liquid conversion process (Li_2S_y to Li_2S_x , $8 \geq x \geq 2$, $8 \geq y \geq 2$), Li_2S_8 symmetric cells were employed for the cyclic voltammetry (CV) measurements. The CNT/B-based cell yielded a higher redox current than the bare CNT-based cell, suggesting enhanced reactivity of the polysulfide on β_{12} -borophene interface (Fig. 3c). The kinetic-regulating role of β_{12} -borophene was subsequently demonstrated in actual Li-S batteries. The CV curves of the as-assembled Li-S batteries exhibited two typical redox peaks, corresponding to the formation of soluble polysulfides (2.2–2.4 V) and solid Li_2S (2.0–2.1 V), respectively. And the two overlapped anodic peaks (2.4–2.6 V) were attributed to the sequential oxidation of Li_2S and polysulfides²⁹. In contrast with the Li-S battery using non-undecorated CNT electrode, the Li-S battery using CNT/B electrode possessed higher current density (Fig. 3d). As shown in Fig. 3e, the Tafel plots of the first oxidation process of the cells using CNT and CNT/B were respectively 57 and 29 mV dec^{-1} , where the smaller Tafel slope of the CNT/B-based cell suggests that the β_{12} -borophene induces higher surface reaction rates. In addition, the simulated interfacial impedance of the Li-S cells sharply decreased from 41.2Ω to 24.9Ω when the electrodes changed from CNT to CNT/B (Fig. 3f), reflecting the β_{12} -borophene was more favorable for the interface electrochemical reactions⁸.

Considering the distinguished electrocatalytic reactivity and polysulfide interactions of the CNT/B-based Li-S battery in the sulfur redox reactions, their actual working performances were further evaluated by regarding the bare CNT-based Li-S battery as a reference. In our experiments, the same amount of polysulfide (Li_2S_8) solution was added as active material (Supplementary Fig. 6). As seen in Fig. 4a, the CV profiles of CNT/B-based battery overlap each other and exhibit excellent reversibility in the redox process, revealing the high-efficiency utilization of sulfur. The galvanostatic charge/discharge profiles are

shown in Fig. 4b. The high reversible specific capacities of 1329, 1236, 1159, 1057, 993, and 919 mAh g⁻¹ were obtained at 0.3, 0.5, 1, 2, 3, and 5 C rates (1 C = 1675 mAh g⁻¹), respectively. Even if the current density increased to 8 C, the CNT/B-based Li-S battery still remained an ultrahigh capacity of 721 mAh g⁻¹. More significantly, after returning current density back to 0.3 C, a reversible capacity of 1216 mAh g⁻¹ recovered immediately with a coulombic efficiency of nearly 100 % (Fig. 4c). By contrast, the battery using bare CNT electrode exhibited inferior rate performances, such as a lower initial capacity of 981 mAh g⁻¹ at 0.3 C and a rapider degradation into 394 mAh g⁻¹ with the increase of capacity to 8 C as well as unsatisfactory capacity restoration after high-rate test (Fig. 4c). As shown in Fig. 4d, the CNT/B-based battery possessed a much lower polarization voltage of 188 mV than the CNT-based battery (217 mV), further revealing the outstanding catalytic property of β_{12} -borophene sheets for polysulfide conversion.

The CNT/B cathode also exhibited excellent cycling stability at current density of 0.5 C, as found in Fig. 4e. The capacity fading rate was only 0.003% per cycle and kept nearly unvaried after 300 cycles when the initial capacity of the CNT/B-based Li-S battery was 1110 mAh g⁻¹. Moreover, the CNT/B-based cell maintained a high coulombic efficiency of ~ 100% in continuous 300 cycle measurements. On the contrary, the bare CNT-based cell delivered a low capacity of 918 mAh g⁻¹ and sharply decreased to 394 mAh g⁻¹ after 300 cycles, resulting in a fast-fading rate of 0.2 % per cycle (Fig. 4e and Supplementary Fig. 7). In addition, both of the high- and low-plateau capacities of CNT/B electrode were much better than bare CNT electrode, demonstrating few-layer β_{12} -borophene sheets can effectively suppress the polysulfide diffusion and improve the polysulfide immobilization (Supplementary Fig. 9)⁵⁶. Moreover, high areal sulfur loadings of 5.3 mg cm⁻² and 7.8 mg cm⁻² with low E/S ratios of 9.8 and 6.8 ml g⁻¹ were respectively performed on the Li-S batteries to test the high-energy density behaviors. It was noted that the areal capacities of the CNT/B-based Li-S cells can reach up to 4.6 and 5.2 mAh cm⁻² when the capacities respectively adopted 871 and 661 mAh g⁻¹ (Fig. 4f), which were much higher than those of 4.0 mAh cm⁻² for commercial Li-ion batteries⁵⁷. Impressively, the CNT/B-based battery could preserve an enough high reversible capacity of 572 mAh g⁻¹ with an extremely-low capacity decay rate of 0.039 % per cycle after 1000 long-term cycles, reflecting excellent cycling stability (Fig. 4g and Supplementary Fig. 8). Notably, the ultralow decay rate and ultrahigh rate performance of 2D β_{12} -borophene sheets are superior to most of other 2D material-based Li-S batteries (Supplementary Table 2), such as phosphorene (785 mAh g⁻¹ at 3 C, decay rate of 0.053% for 1000 cycles)³⁰, C₃N₄ (340 mAh g⁻¹ at 4 C, decay rate of 0.5% for 200 cycles)⁵⁸, and graphene (700 mAh g⁻¹ at 2 C, decay rate of 0.5% for 70 cycles)⁵⁹.

Finally, we calculated the adsorption energy of soluble polysulfides on a monolayer β_{12} -borophene using DFT calculation to comprehend the improvement mechanism of β_{12} -borophene sheets on Li-S batteries, as observed in Supplementary Fig. 10. Figure 5a gives the optimized configurations of S₈ and Li₂S_n on monolayer β_{12} -borophene sheet. Based on the DFT calculations, S₈ has the weakest adsorption energy on borophene of only 1.23 eV among all configurations, and the adsorption energy gradually increases with the progression of the polysulfides' lithiation and eventually arrives at 3.8 eV for the fully-lithiated Li₂S

(Fig. 5b). The adsorption energy of polysulfides on β_{12} -borophene is far higher than that on CNT (below 1 eV), unveiling that β_{12} -borophene can anchor polysulfide and inhibit the shuttle of lithium polysulfide more effectively than CNT. Figure 5c shows the typical partial density of states (PDOS) of Li_2S_4 on monolayer β_{12} -borophene, and more details can be seen in Supplementary Fig. 11. The 2p orbital electrons of Li_2S_4 and β_{12} -borophene were found to overlap near the Fermi level, suggesting the formation of a strong chemical bonding between β_{12} -borophene and Li_2S_4 cluster. This is probably originated from a strong charge transfer of 0.22 e from β_{12} -borophene to Li_2S_4 cluster (Fig. 5d) based on the charge density difference and bader charge analysis. The strong chemical interaction between β_{12} -borophene and Li_2S_4 cluster can be also ascertained because the dark-yellow color of Li_2S_4 solution will gradually attenuate with the increase of the mixing time with β_{12} -borophene (Supplementary Fig. 12). Furthermore, the diffusion barrier of Li^+ on β_{12} -borophene was deduced to be only 0.10 eV (Fig. 5e), much lower than that (0.28 eV) on CNT (Supplementary Fig. 13). The enhanced surface migration of Li^+ on borophene would further accelerate the nucleation and decomposition of Li_2S_n and thus improves the capacity and charge-discharge rate of Li-S battery⁶⁰.

In summary, we have developed a novel, facile and high-yield LTLE strategy to produce single crystalline few-layer β_{12} -borophene sheets. As promising 2D electrode materials, the β_{12} -borophene sheets were firstly used as efficient polysulfide-conversion electrocatalysts for Li-S batteries. Due to the usage of few-layer β_{12} -borophene sheets, the CNT/B-based Li-S batteries exhibited a high areal sulfur loading of 5.2 mgh cm^{-2} at 7.8 mg cm^{-2} under a low E/S ratio of 6.8 ml g^{-1} at 0.3 C. Compared with the CNT-based Li-S cell, the CNT/B-based Li-S cell exhibited a better rate performance of as high as 721 mAh g^{-1} at 8 C and a much lower decay rate of only 0.039 % in 1000 cycles. By DFT calculations, β_{12} -borophene had a lower surface diffusion barrier of Li ion and a stronger adsorption for Li_2S_n clusters than CNT, which can effectively inhibit the shuttle effect of polysulfides and accelerate their decomposition at the same time. These should be responsible for the extraordinary catalytic activity of β_{12} -borophene towards polysulfides in the CNT/B-based Li-S cell. Therefore, our strategy will pave a new way for the design of high-energy rechargeable batteries through the exploration of 2D boron-based nanomaterials.

Methods

Synthesis of few-layer β_{12} -borophene sheets. The low-temperature liquid exfoliation (LTLE) method was firstly developed to synthesize β_{12} -borophene sheets at milligram scale by using boron powder (99.8 %, Zhongnuo Incorp., China) as source materials. Firstly, 20 ~ 50 mg boron powers were added into 50 ml N,N-Dimethylformamide (NMP, 99.9 %, Innochem. Incorp., China) to form uniform and well-dispersed solution by several minutes' stirring, as seen in Figure S1. Secondly, the boron-power solution was transferred into the ethanol path and treated at -20~-25 °C in the tip-type ultrasonicator equipped with cooling system (SXSONIC Incorp., China), where the ultrasonic power was kept at 800 W and the treatment lasted for 4 ~ 8 h. Thirdly, the product solution was statically settled at room temperature for 48 ~ 72 h to enough precipitate the undissolved boron powder. Finally, the suspension was centrifuged at

about 10000 ~ 11000 revolutions per minute (rpm) for 30 minutes to obtain solid products. After the above synthesis process, the mass of the collected 2D sheets was ranging from 4 to 10 mg. Accordingly, the yield of 2D few-layer borophene by LTLE way can reach as high as over 20 %, which is much higher than those by many other methods in previous reports (Supplementary Table 1) ^{48,49}.

Material characterizations. The morphology of β_{12} -borophene sheets was investigated by SEM (Zeiss Supra 60) and AFM (Bruker Dimension Fastscan). XPS (ThermoFisher Nexsa), XRD (D-MAX 2200 VPC) and Raman spectroscopy (inVia Reflex, 532-nm laser) were respectively used to analyze the chemical compositions of the sample. UV-vis spectroscopy (UV-3600) was applied to determine the energy-band structure and absorption coefficient of β_{12} -borophene sheets. TEM and HRTEM (FEI Titan 80–300) were employed to ascertain the lattice structure of the product. The STEM and elemental mapping were performed on a JEM ARM200F thermal-field emission microscope with a probe Cs-corrector working at 200 kV. For the HAADF imaging, the convergence angle of ~ 23 mrad and collection angle range of 68 ~ 174 mrad were adopted for the incoherent atomic number imaging. Both the elemental composition and distribution were analyzed on the energy dispersive X-ray analyzer (EDS, EX-230 100m² detector) equipped with the microscope.

Preparation of Li₂S₈ catholyte. The sources of sulfur and Li₂S with a molar ratio of 7:1 were put into an appropriate amount of 1 mol l⁻¹ lithium bis (trifluoromethanesulfonyl) imide (LiTFSI). Secondly, the LiTFSI solution was added into the mixed solvent of 1,3-dioxolane (DOL) and 1,2-dimethoxyethane (DME) (volume ratio (v:v): 1:1). Thirdly, 1 wt.% LiNO₃ was used as additive by vigorous magnetic stirring at 50 °C until the sulfur powder were fully dissolved. The concentration of Li₂S₈ was ranging from 0.15 to 2 mol l⁻¹.

Fabrication of CNT electrodes. 5 g commercial multiwalled CNT (length ~ 50 nm, Aladdin, China) powders were dispersed into 50 ml Triton X-100 aqueous solution (0.01 wt.%, Secco Romeo, China) to form uniform and homodisperse solution by ultrasonication for 2 h. Subsequently, the obtained CNT solution was filtered through nylon film under vacuum. After three-time washing by deionized water and drying for 2 h at 60 °C in vacuum oven, the free-standing CNT paper was peeled from the nylon film. Finally, the obtained CNT paper was cut into desired disks as the free-standing electrode.

Assembly of symmetric cells for kinetic evaluation of polysulfide conversion. CNT/B (with a mass loading of about 1 mg β_{12} -borophene sheets) or bare CNT electrodes were used as both working and counter electrodes. And 40 μ l catholyte (0.5 mol l⁻¹ Li₂S₆ and 1.0 mol l⁻¹ solution of LiTFSI with 1 wt.% LiNO₃ in DOL and DME, v/v = 1:1) was added into each coin cell. The CV behaviors of the symmetric cell were tested at a scan rate of 10 mV s⁻¹, in which the voltage window ranged from - 0.8 to 0.8 V.

Measurement on the nucleation and dissolution of Li₂S. The CNT/B or CNT film electrodes were used as cathodes and Li foils were employed as the anodes. Also, 20 μ l Li₂S₈ solution (0.15 mol l⁻¹) was applied as catholyte, and 20 μ l electrolyte without Li₂S₈ was used as anolyte. For the nucleation and growth of

Li₂S, the assembled cells were first discharged galvanostatically to 2.06 V at 0.112 mA, and then discharged potentiostatically to 2.05 V until the current dropped to below 10⁻⁵ A. The deposition capacities of Li₂S were calculated according to the Faraday's law. For the Li₂S dissolution, the assembled cells were firstly galvanostatically discharged to 1.80 V at 0.10 mA, and subsequently galvanostatically discharged to 1.80 V at 0.01 mA for fully transforming sulfur species into solid Li₂S. Then the cells were potentiostatically charged at 2.40 V to oxidize Li₂S into soluble polysulfides. The potentiostatic charge was accomplished when the charge current was below 10⁻⁵ A.

Assembly and performance evaluation of Li-S cells. CR-2016 coin cells were assembled in an argon-protected glove box, where the CNT/B or CNT films were employed as the cathodes and 20 μl Li₂S₈ catholyte was dropped onto the CNT film as the sulfur cathode. Also, Li foil was applied as the counter electrode, and 1.0 M solution of LiTFSI with 1 wt.% LiNO₃ in DOL and DME (v/v= 1:1) was used as the electrolyte. In experiments, the common areal loading of sulfur was about 1 mg cm⁻², and the electrolyte/sulfur ratio was fixed at 15 μl mg⁻¹. The electrochemical performances of Li-S batteries were measured by a LANDCT2001A analyzer, where the voltage interval ranged from 1.7 to 2.8 V. And the cyclic voltammograms (CV) curves were collected at 0.1 mV s⁻¹ on a CHI-760E electrochemical workstation (Chenhua Instrument, Shanghai), in which EIS analysis was in the range of 10 kHz-0.01 Hz.

Theoretical model of few-layer β₁₂-borophene sheets. All the calculations except superconducting properties were carried out using Vienna *ab initio* simulation package (VASP 5.4)^{61,62} with projector augmented wave (PAW) pseudopotential method^{63,64} and Perdew-Burke-Ernzerhof (PBE) functional⁶⁵. Both lattice parameters and atomic positions were optimized by conjugate gradient method, and the convergence criteria for energy and force were eV and eVÅ⁻¹, respectively. The kinetic energy cutoff for plane waves was set at 450 eV. The Brillouin zones were sampled with Å⁻¹ spacing in reciprocal space by the Monkhorst-Pack scheme⁶⁶. The high symmetry K-points for band structure and phonon dispersion curves were generated by AFLOW package⁶⁷. And Grimme's DFT-D3 van der Waals corrections with the Becke-Jonson damping^{68,69} was employed. The phonon spectrum was calculated by DFPT method implemented in Phonopy program⁶⁹. Also, the crystal structures were visualized by VESTA package⁷⁰.

Computational methods of the adsorption energy of few-layer β₁₂-borophene. First-principle calculations were implemented using VASP⁶¹ software package. The PBE⁶⁵ functional of generalized gradient approximation (GGA) was used for the exchange-correlation. The basis set utilized PAW pseudopotential method^{63,64}, and the energy cutoff was set at 400 eV. The self-consistent field (SCF) tolerance was eV and the force convergence criterion for atomic relaxation was 0.02 eV Å⁻¹. A Monkhorst-Pack k-point mesh with different sizes was chosen to meet various requirements, where is for the geometrical relaxation, is for the calculation of electronic structure and is for the calculation of adsorption. The vdW forces between Li₂S_n and β₁₂-borophene sheet or CNT were accurately obtained by the DFT-D3 method⁶⁸. The supercell of β₁₂-borophene and

CNT was used for the adsorption energy and CI-NEB calculations, respectively. The adsorption energy () was derived using the following equation:

In this equation, E_{sub} , $E_{Li_2S_n/S_8}$, and $E_{sub@Li_2S_8/S_8}$ represent the energy of free β_{12} -borophene or CNT supercell substrate, the energy of free Li_2S_n or S_8 species, and the energy of β_{12} -borophene or CNT substrate after the adsorption of polysulphide species, respectively. Positive energy values suggest the kinetically stable adsorption of Li_2S_n or S_8 on the substrate, and higher adsorption energy implies the adsorption sites are energy favorable.

Data availability

The authors declare that all the data supporting the findings of this study are available within the article and its Supplementary Information or from the corresponding authors upon reasonable request.

Declarations

Acknowledgements

The authors are very thankful for the support of the National Science Foundation of China (Grant Nos. 51872337, 51872283, 22075279, 21872145), National Project for the Development of Key Scientific Apparatus of China (2013YQ12034506), National Key Research and Development Program of China (Grant no. 2019YFA0210203, 2016YFB0100100, 2016YFA0200200), the Fundamental Research Funds for the Central Universities of China, the Science and Technology Department of Guangdong Province and the Education Department of Guangdong Province, the Liao Ning Revitalization Talents Program (Grant XLYC1807153), the Natural Science Foundation of Liaoning Province, Joint Research Fund Liaoning-Shenyang National Laboratory for Materials Science (Grant 20180510038), Dalian Science and Technology Bureau (2019RT09), Dalian National Laboratory For Clean Energy (DNL), CAS, DNL Cooperation Fund, CAS (DNL180310, DNL180308, DNL201912, and DNL201915), DICP (DICP ZZBS201708, DICP ZZBS201802, DICP I2020032), DICP&QIBEBT (Grant DICP&QIBEBT UN201702), GFKJCXTQ Foundation (Grant 18-163-14-ZT-002-001-02).

Author contributions

B. Y., Z. -S. W. and F. L. proposed and supervised the projects. H.J.L. synthesized the borophene sheets, and characterized their surface morphology and chemical compositions. H. D. S. fabricated the CNT- and CNT/B-based Li-S batteries, and carried out the electrochemical measurements. Z. W. carried out the TEM analysis of the borophene sheets and calculated the adsorption energies of Li_2S_n clusters on monolayer borophene or CNT by DFT model. Y. W. M. proposed the DFPT model of the surface configuration of the β_{12} -borophene. H. J. L., H. D. S, Z. W., Y. W. M., S. D. L., B. Y., Z. -S. W. and F. L. wrote the paper. All the authors involved in the analysis and discussion of the experimental results. And all authors approve to submit the final version of the manuscript.

Additional information

Supplementary Information accompanies this paper at <http://www.nature.com/naturecommunications>

Competing financial interests: The authors declare no competing financial interests

Reprints and permission information is available online at <http://npg.nature.com/reprintsandpermissions/>

Publisher's note: Springer Nature remains neutral with regard to jurisdictional claims in published maps and institutional affiliations

References

1. Kang, K., Meng, Y. S., Breger, J., Grey, C. P. & Ceder, G. Electrodes with High Power and High Capacity for Rechargeable Lithium Batteries. *Science* **311**, 977–980 (2006).
2. Choi, J. W. & Aurbach, D. Promise and reality of post-lithium-ion batteries with high energy densities. *Nat. Rev. Mater.* **1**, 16013 (2016).
3. Bruce, P. G., Freunberger, S. A., Hardwick, L. J. & Tarascon, J. M. Li-O₂ and Li-S batteries with high energy storage. *Nat. Mater.* **11**, 19–29 (2012).
4. Shi, H. *et al.* A Two-Dimensional Mesoporous Polypyrrole-Graphene Oxide Heterostructure as a Dual-Functional Ion Redistributor for Dendrite-Free Lithium Metal Anodes. *Angew. Chem. Int. Ed.* **59**, 12147–12153 (2020).
5. Xu, Z. L. *et al.* Exceptional catalytic effects of black phosphorus quantum dots in shuttling-free lithium sulfur batteries. *Nat. Commun.* **9**, 4164 (2018).
6. Lin, D., Liu, Y. & Cui, Y. Reviving the lithium metal anode for high-energy batteries. *Nat. Nanotechnol.* **12**, 194 (2017).
7. Peng, H. J., Huang, J. Q. & Q. Zhang. A review of flexible lithium-sulfur and analogous alkali metal-chalcogen rechargeable batteries. *Chem. Soc. Rev.* **46**, 5237 (2017).
8. Boyjoo, Y. *et al.* Molecular-Level Design of Pyrrhotite Electrocatalyst Decorated Hierarchical Porous Carbon Spheres as Nanoreactors for Lithium-Sulfur Batteries. *Adv. Energy Mater.* **10**, 2000651

- (2020).
9. Shi, H. *et al.* Dual-Functional Atomic Zinc Decorated Hollow Carbon Nanoreactors for Kinetically Accelerated Polysulfides Conversion and Dendrite Free Lithium Sulfur Batteries. *Adv. Energy Mater.* **10**, 2002271 (2020).
 10. Knoop, J. E. & Ahn, S. Recent advances in nanomaterials for high-performance Li–S batteries. *J. Energy Chem.* **47**, 86 (2020).
 11. Bhargava, A., He, J., Gupta, A. & Manthiram, A. Lithium-Sulfur Batteries: Attaining the Critical Metrics. *Joule* **4**, 285 (2020).
 12. Liang, J., Sun, Z. H., Li, F. & Cheng, H. M. Carbon materials for Li-S batteries: Functional evolution and performance improvement. *Energy Storage Mater.* **2**, 76–106 (2016).
 13. Tao, Y. *et al.* Kinetically-enhanced polysulfide redox reactions by Nb₂O₅ nanocrystals for high-rate lithium-sulfur battery. *Energy Environ. Sci.* **9**, 3230–3239 (2016).
 14. Liang, X. *et al.* Tuning Transition Metal Oxide-Sulfur Interactions for Long Life Lithium Sulfur Batteries: The "Goldilocks" Principle. *Adv. Energy Mater.* **6**, 1501636 (2016).
 15. He, J. *et al.* Freestanding 1T MoS₂/graphene heterostructures as a highly efficient electrocatalyst for lithium polysulfides in Li–S batteries. *Energy Environ. Sci.* **12**, 344 (2019).
 16. Liu, X., Huang, J. Q., Zhang, Q. & Mai, L. Nanostructured Metal Oxides and Sulfides for Lithium-Sulfur Batteries. *Adv. Mater.* **29**, 1601759 (2017).
 17. Zhou, G. *et al.* Catalytic oxidation of Li₂S on the surface of metal sulfides for Li-S batteries. *npj 2D Mater. Appl.* **114**, 840–845 (2017).
 18. Cai, W. *et al.* Conductive Nanocrystalline Niobium Carbide as High-Efficiency Polysulfides Tamer for Lithium-Sulfur Batteries. *Adv. Funct. Mater.* **28**, 1704865 (2018).
 19. Luo, L., Chung, S. H., Asl, H. Y. & Manthiram, A. Long-Life Lithium-Sulfur Batteries with a Bifunctional Cathode Substrate Configured with Boron Carbide Nanowires. *Adv. Mater.* **30**, 1804149 (2018).
 20. Shi, H. *et al.* Free-standing integrated cathode derived from 3D graphene/carbon nanotube aerogels serving as binder-free sulfur host and interlayer for ultrahigh volumetric-energy-density lithium sulfur batteries. *Nano Energy* **60**, 743–751 (2019).
 21. Lim, W. G. *et al.* Approaching Ultrastable High-Rate Li-S Batteries through Hierarchically Porous Titanium Nitride Synthesized by Multiscale Phase Separation. *Adv. Mater.* **31**, 1806547 (2019).
 22. Sun, Z. *et al.* Conductive porous vanadium nitride/graphene composite as chemical anchor of polysulfides for lithium-sulfur batteries. *Nat. Commun.* **8**, 14627 (2017).
 23. Wang, Y. *et al.* Carbon@titanium nitride dual shell nanospheres as multi-functional hosts for lithium sulfur batteries. *Energy Storage Mater.* **16**, 228–235 (2019).
 24. Li, R., Zhou, X., Shen, H., Yang, M. & Li, C. Conductive Holey MoO₂–Mo₃N₂ Heterojunctions as Job-Synergistic Cathode Host with Low Surface Area for High-Loading Li–S Batteries. *Acs Nano* **13**, 10049–10061 (2019).

25. Chen, M. *et al.* Multifunctional Heterostructures for Polysulfide Suppression in High-Performance Lithium-Sulfur Cathode. *Small* **14**, 1803134 (2018).
26. Yao, Y. *et al.* A Dual-Functional Conductive Framework Embedded with TiN-VN Heterostructures for Highly Efficient Polysulfide and Lithium Regulation toward Stable Li-S Full Batteries. *Adv. Mater.* **32**, 1905658 (2020).
27. Shao, Q., Wu, Z. & Chen, J. Two-dimensional materials for advanced Li-S batteries. *Energy Storage Mater.* **22**, 284–310 (2019).
28. Dong, Y. *et al.* 2D hierarchical yolk-shell heterostructures as advanced host-interlayer integrated electrode for enhanced Li-S batteries. *J. Energy Chem.* **36**, 64–73 (2019).
29. Wang, Y. *et al.* Highly Stable Lithium – Sulfur Batteries Promised by Siloxene: An Effective Cathode Material to Regulate the Adsorption and Conversion of Polysulfides. *Adv. Funct. Mater.* **30**, 1910331 (2020).
30. Li, L. *et al.* Phosphorene as a Polysulfide Immobilizer and Catalyst in High-Performance Lithium-Sulfur Batteries. *Adv. Mater.* **29**, 1602734 (2017).
31. Xu, Z. *et al.* Exceptional catalytic effects of black phosphorus quantum dots in shuttling-free lithium sulfur batteries. *Nat. Commun.* **9**, 4164 (2018).
32. Fan, Y. *et al.* Functionalized Boron Nitride Nanosheets/Graphene Interlayer for Fast and Long-Life Lithium-Sulfur Batteries. *Adv. Energy Mater.* **7**, 1602380 (2017).
33. Kim, P. J. H. *et al.* Synergistic protective effect of a BN-carbon separator for highly stable lithium sulfur batteries. *NPG Asia Mater.* **9**, e375 (2017).
34. Jia, Z. *et al.* Trithiocyanuric acid derived g-C₃N₄ for anchoring the polysulfide in Li-S batteries application. *J. Energy Chem.* **43**, 71–77 (2020).
35. Zhang, J. *et al.* Microemulsion Assisted Assembly of 3D Porous S/Graphene@g-C₃N₄ Hybrid Sponge as Free-Standing Cathodes for High Energy Density Li-S Batteries. *Adv. Energy Mater.* **8**, 1702839 (2018).
36. Dong, Y. *et al.* All-MXene-Based Integrated Electrode Constructed by Ti₃C₂ Nanoribbon Framework Host and Nanosheet Interlayer for High-Energy-Density Li-S Batteries. *ACS Nano* **12**, 2381–2388 (2018).
37. Tang, H. *et al.* A Robust, Freestanding MXene-Sulfur Conductive Paper for Long-Lifetime Li-S Batteries. *Adv. Funct. Mater.* **29**, 1901907 (2019).
38. Rao, D. *et al.* Ultrahigh energy storage and ultrafast ion diffusion in borophene-based anodes for rechargeable metal ion batteries. *J. Mater. Chem. A* **5**, 2328–2338 (2017).
39. Zhang, Y., Wu, Z. F., Gao, P. F., Zhang, S. L. & Wen, Y. H. Could Borophene Be Used as a Promising Anode Material for High-Performance Lithium Ion Battery? *ACS Appl. Mater. Interfaces* **8**, 22175–22181 (2016).
40. Rao, D. *et al.* Interfacial competition between a borophene-based cathode and electrolyte for the multiple-sulfide immobilization of a lithium sulfur battery. *J. Mater. Chem. A* **7**, 7092–7098 (2019).

41. Liang, X., Rangom, Y., Kwok, C. Y., Pang, Q. & Nazar, L. F. Interwoven MXene Nanosheet/Carbon-Nanotube Composites as Li-S Cathode Hosts. *Adv. Mater.* **29**, 1603040 (2017).
42. Mannix, A. J., Zhang, Z., Guisinger, N. P., Yakobson, B. I. & Hersam, M. C. Borophene as a prototype for synthetic 2D materials development. *Nat. Nanotechnol.* **13**, 444–450 (2018).
43. Wang, Z., Lu, T., Wang, H., Feng, Y. & Zheng, J. High anisotropy of fully hydrogenated borophene. *Phys. Chem. Chem. Phys.* **18**, 31424–31430 (2016).
44. Tian, Y. *et al.* Inorganic Boron-Based Nanostructures: Synthesis, Optoelectronic Properties, and Prospective Applications. *Nanomaterials* **9**, 538 (2019).
45. Lherbier, A., Botello Méndez, A. R. & Charlier, J. C. Electronic and optical properties of pristine and oxidized borophene. *2D Mater.* **3**, 045006 (2016).
46. Xu, S. *et al.* Two-Dimensional Semiconducting Boron Monolayers. *J. Am. Chem. Soc.* **139**, 17233–17236 (2017).
47. Wang, Z. Q., Lü, T. Y., Wang, H. Q., Feng, Y. P. & Zheng, J. C. Review of borophene and its potential applications. *Front. Phys.* **14**, 33403 (2019).
48. Ji, X. *et al.* A Novel Top-Down Synthesis of Ultrathin 2D Boron Nanosheets for Multimodal Imaging-Guided Cancer Therapy. *Adv. Mater.* **30**, 1803031 (2018).
49. Fan, Q. *et al.* High-yield production of few-layer boron nanosheets for efficient electrocatalytic N₂ reduction. *Chem. Commun.* **55**, 4246–4249 (2019).
50. Zhang, C. *et al.* Cryogenic Exfoliation of Non-layered Magnesium into Two-Dimensional Crystals. *Angew. Chem. Int. Ed.* **58**, 8814–8818 (2019).
51. Feng, B. *et al.* Experimental realization of two-dimensional boron sheets. *Nat. Chem.* **8**, 564–569 (2016).
52. Li, H. *et al.* Scalable Production of Few-Layer Boron Sheets by Liquid-Phase Exfoliation and Their Superior Supercapacitive Performance. *ACS Nano* **12**, 1262–1272 (2018).
53. Hernandez, Y. *et al.* High-yield production of graphene by liquid-phase exfoliation of graphite. *Nat. Nanotechnol.* **3**, 563–568 (2008).
54. Xing, C. *et al.* 2D Nonlayered Selenium Nanosheets: Facile Synthesis, Photoluminescence, and Ultrafast Photonics. *Adv. Optical Mater.* **5**, 1700884 (2017).
55. Sheng, S. *et al.* Raman Spectroscopy of Two-Dimensional Borophene Sheets. *ACS Nano* **13**, 4133–4139 (2019).
56. Tu, S. *et al.* A Polysulfide-Immobilizing Polymer Retards the Shuttling of Polysulfide Intermediates in Lithium-Sulfur Batteries. *Adv. Mater.* **30**, 1804581 (2018).
57. Xiao, B. & Sun, X. Surface and Subsurface Reactions of Lithium Transition Metal Oxide Cathode Materials: An Overview of the Fundamental Origins and Remedying Approaches. *Adv. Energy Mater.* **8**, 1802057 (2018).
58. Huangfu, Y. *et al.* Facile fabrication of permselective g-C₃N₄ separator for improved lithium-sulfur batteries. *Electrochim. Acta* **272**, 60–67 (2018).

59. Fei, L. *et al.* Graphene/Sulfur Hybrid Nanosheets from a Space-Confined "Sauna" Reaction for High-Performance Lithium-Sulfur Batteries. *Adv. Mater.* **27**, 5936–5942 (2015).
60. Zhang, L. *et al.* Borophene as Efficient Sulfur Hosts for Lithium–Sulfur Batteries: Suppressing Shuttle Effect and Improving Conductivity. *J. Phys. Chem. C* **121**, 15549–15555 (2017).
61. Kresse, G. & Furthmüller, J. Efficient iterative schemes for ab initio total-energy calculations using a plane-wave basis set. *Phys. Rev. B* **54**, 11169–11186 (1996).
62. Kresse, G. & Hafner, J. Norm-conserving and ultrasoft pseudopotentials for first-row and transition elements. *J. Phys. Condens. Matter* **6**, 8245–8257 (1994).
63. Blöchl, P. E. Projector augmented-wave method. *Phys. Rev. B* **50**, 17953–17979 (1994).
64. Kresse, G. & Joubert, D. From ultrasoft pseudopotentials to the projector augmented-wave method. *Phys. Rev. B* **59**, 1758–1775 (1999).
65. Perdew, J. P., Burke, K. & Ernzerhof, M. Generalized gradient approximation made simple. *Phys. Rev. Lett.* **77**, 3865–3868 (1996).
66. Monkhorst, H. J. & Pack, J. D. Special points for Brillouin-zone integrations. *Phys. Rev. B* **13**, 5188–5192 (1976).
67. Curtarolo, S. *et al.* AFLOW: An automatic framework for high-throughput materials discovery. *Comput. Mater. Sci.* **58**, 218–226 (2012).
68. Grimme, S., Antony, J., Ehrlich, S. & Krieg, H. A consistent and accurate ab initio parametrization of density functional dispersion correction (DFT-D) for the 94 elements H-Pu. *J. Chem. Phys.* **132**, 154104 (2010).
69. Sun, G., Li, Y., Zhao, X., Mi, Y. & Wang, L. First-Principles Investigation of the Effect of M-Doped (M = Zr, Hf) TiCoSb Half-Heusler Thermoelectric Material. *J. Mater. Sci. Chem. Eng.* **03**, 78–86 (2015).
70. Momma, K. & Izumi, F. VESTA 3 for three-dimensional visualization of crystal, volumetric and morphology data. *J. Appl. Crystallogr.* **44**, 1272–1276 (2011).

Figures

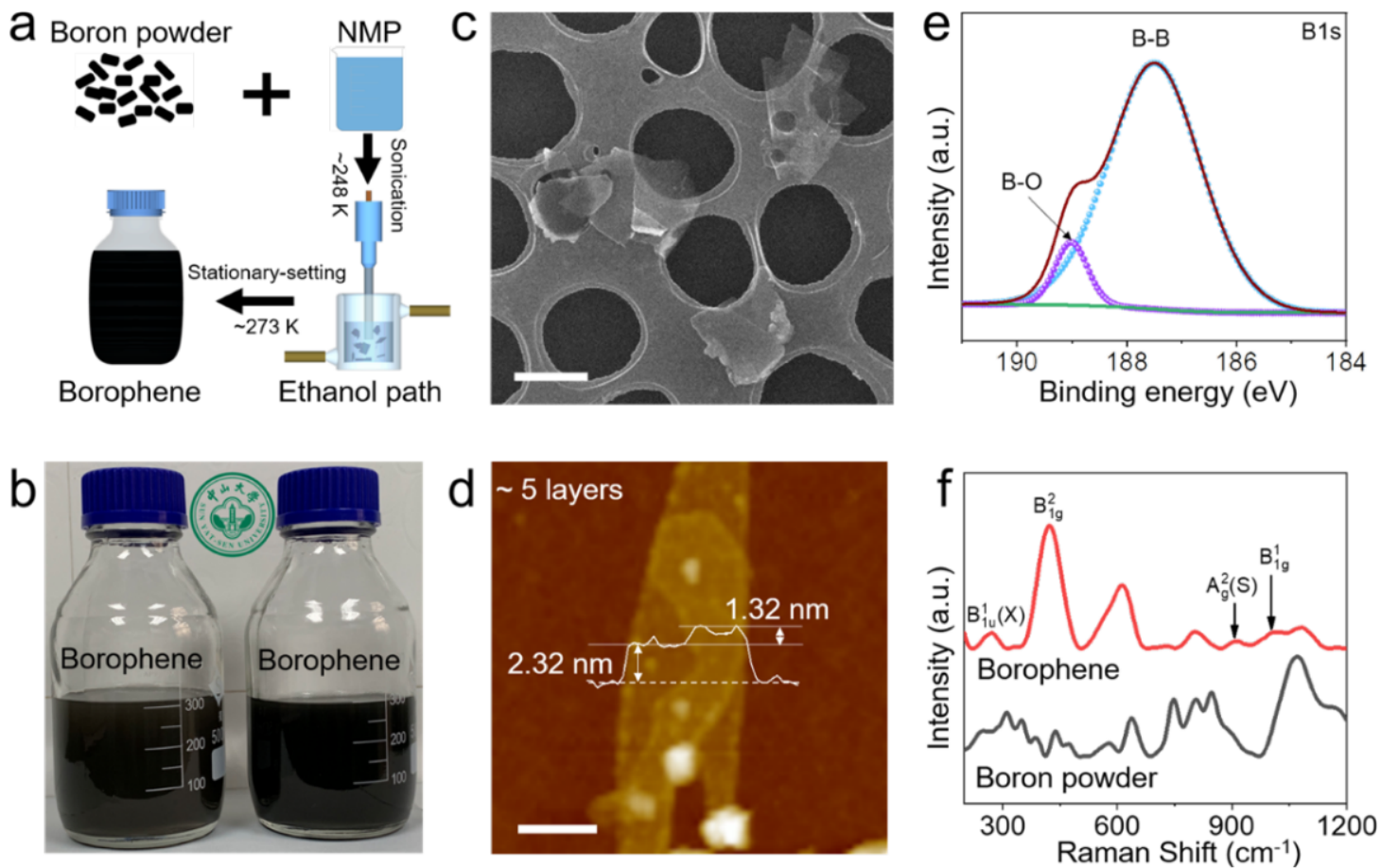


Figure 1

Synthesis process and characterization of 2D few-layer borophene sheets. (a) Schematic diagram of the LTLE process of 2D few-layer borophene sheets. (b) Photograph of 2D borophene sheets in NMP solution. (c, d) SEM and AFM images of 2D borophene sheets, respectively. (e) Typical XPS spectrum and peak deconvolution of borophene sheets. (f) Raman spectra of pristine boron powder and 2D borophene sheets. Scale bar: (c) $2 \mu\text{m}$, and (d) 100 nm .

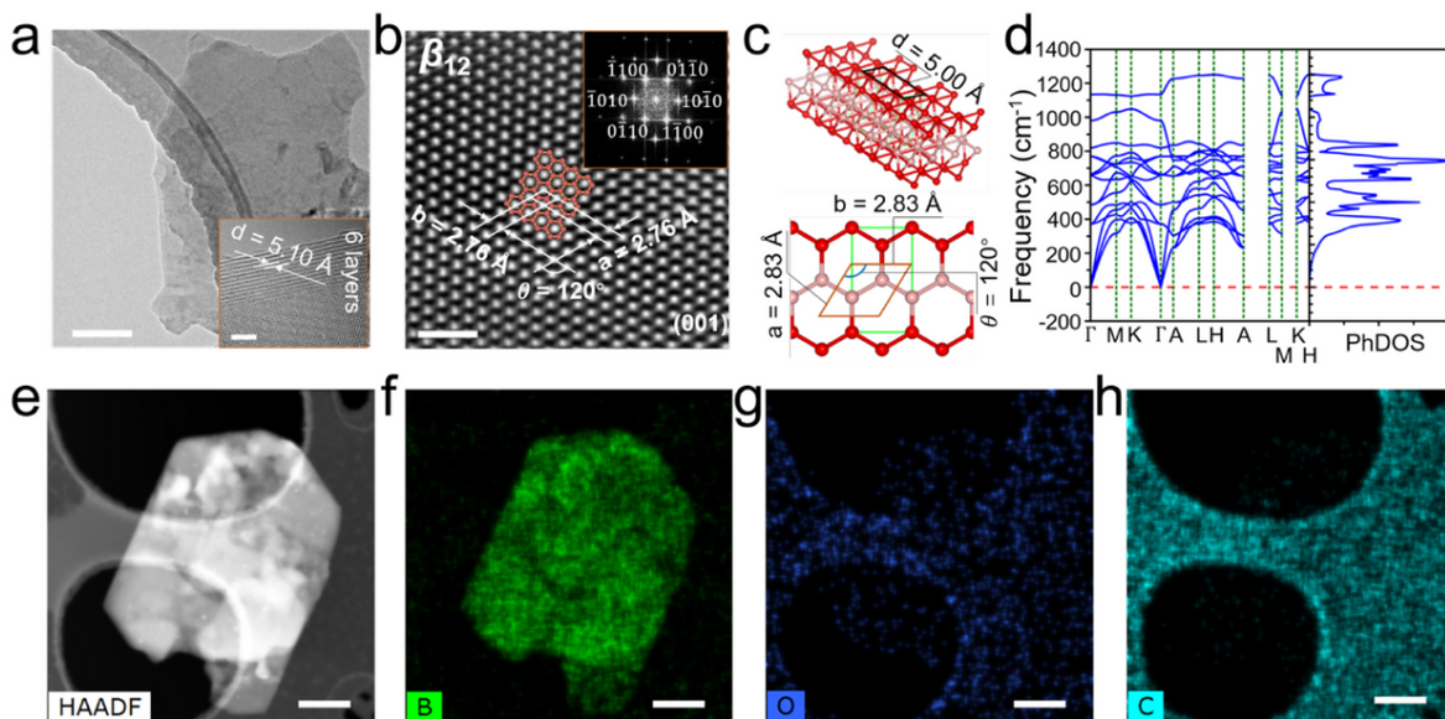


Figure 2

Surface configuration of few-layer borophene. (a) TEM image of a 2D borophene sheet (scale bar: 200 nm). The inset presents the cross-sectional image of a few-layer sheet (scale bar: 2 nm). (b) Typical HRTEM image of the borophene sheet (scale bar: 1 nm). The corresponding selected area electron diffraction (SAED) pattern is shown as the inset. (c) Side and top views of the β_{12} -B5 allotrope labelled with lattice parameters by DFT model. (d) Phonon dispersion curves and density of states (PhDOS) for the β_{12} -B5 allotrope based on DFPT method. (e) HAADF-STEM image of a borophene sheet. (f-h) The corresponding EDX element-mapping images of B, O and C, respectively (scale bar: 500 nm).

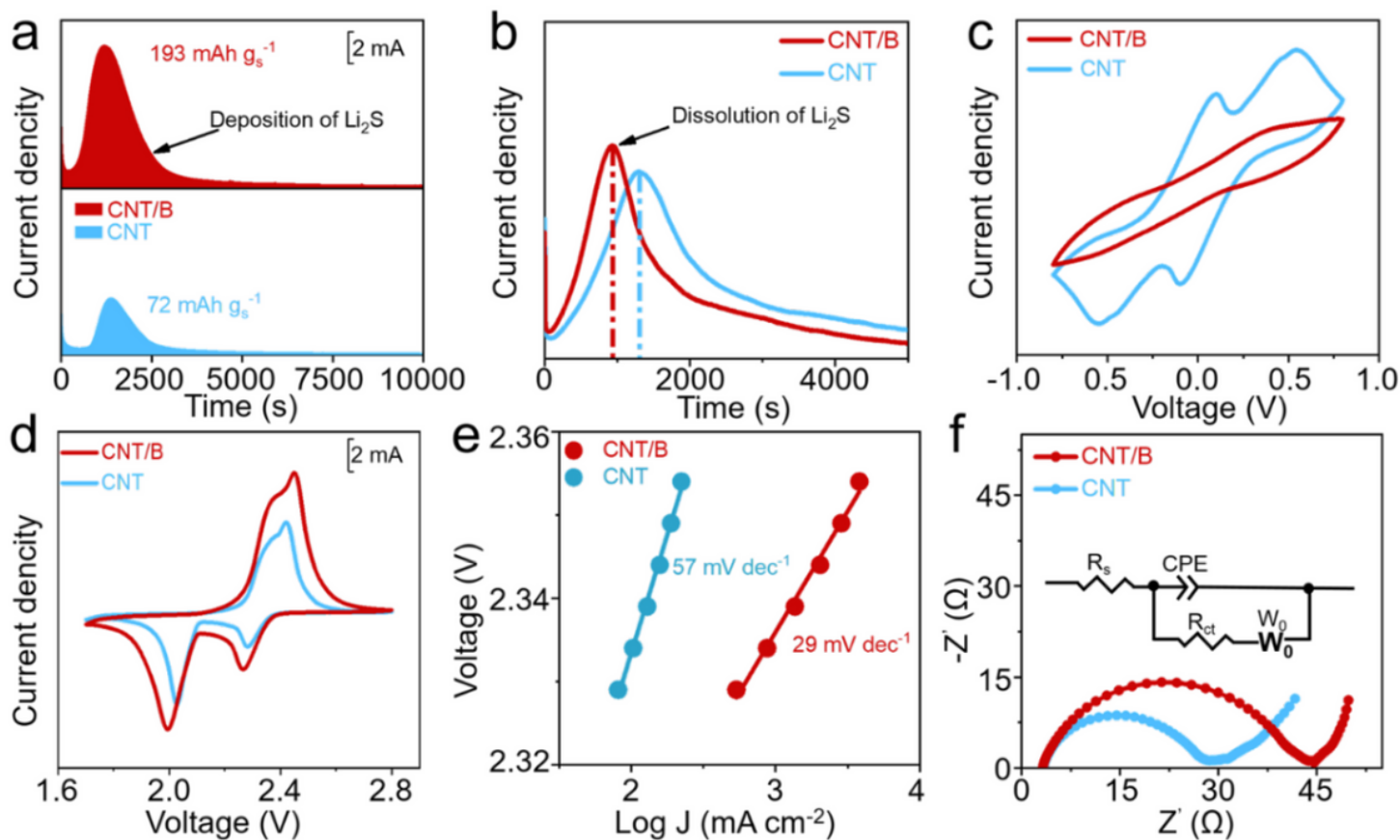


Figure 3

Electrocatalytic activity of borophene sheets for polysulfides. (a) Potential static discharge curves of the $\text{Li}_2\text{S}_8/\text{tetraglyme}$ solution using CNT/B and CNT electrodes at 2.05 V, respectively. (b) Potentiostatic charge profiles of the CNT/B and CNT electrodes at 2.40 V to evaluate dissolution behaviors of Li_2S . (c) CV curves of Li_2S_6 symmetric batteries employing CNT/B and CNT electrode at 5 mV s^{-1} . (d) CV curve comparisons of the cells using CNT/B and CNT electrodes as sulfur hosts at a scan rate of 1 mV s^{-1} . (e) Corresponding Tafel plots for the oxidation peaks, and (f) Nyquist plots of Li-S batteries using CNT/B and CNT cathodes, respectively.

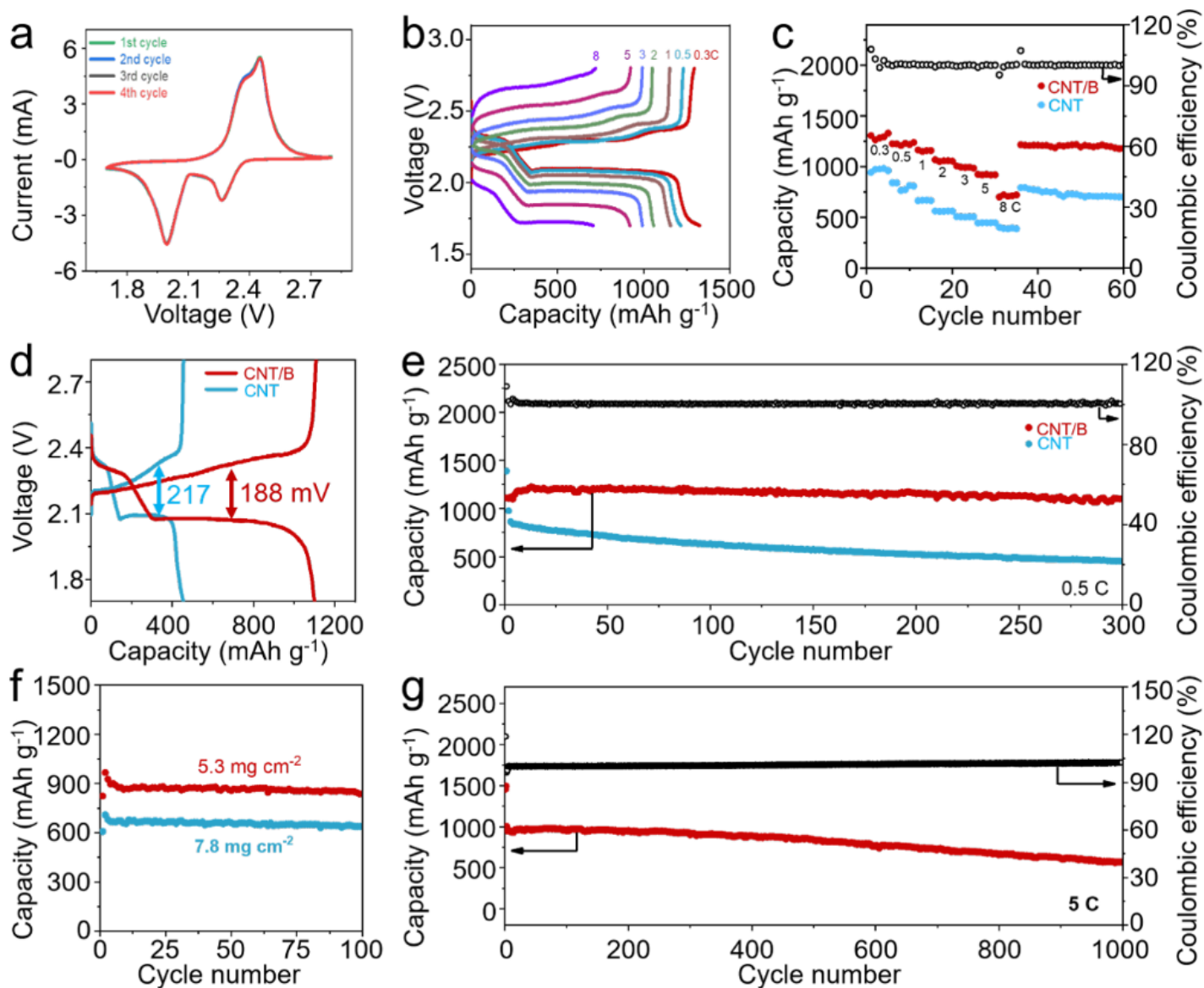


Figure 4

Electrochemical performances of the CNT- and CNT/B-based Li-S batteries. (a) CV curves of the Li-S battery using CNT/B electrode at a scan rate of 0.1 mV s⁻¹. (b) The galvanostatic charge/discharge curves of the CNT/B-based Li-S battery at different rates. (c) The rate performances of the Li-S batteries using bare CNT and CNT/B cathodes. (d) Galvanostatic charge/discharge profiles at 0.5 C. (e) Cycling stability and coulombic efficiency of the CNT- and CNT/B-based batteries at 0.5 C, respectively. (f) Cycling performances of the CNT/B-based batteries with high sulfur loading of 5.3 and 7.8 mg cm⁻² at 0.3 C. (g) Long-term cycling stability and coulombic efficiency of the CNT/B-based Li-S battery at 5 C.

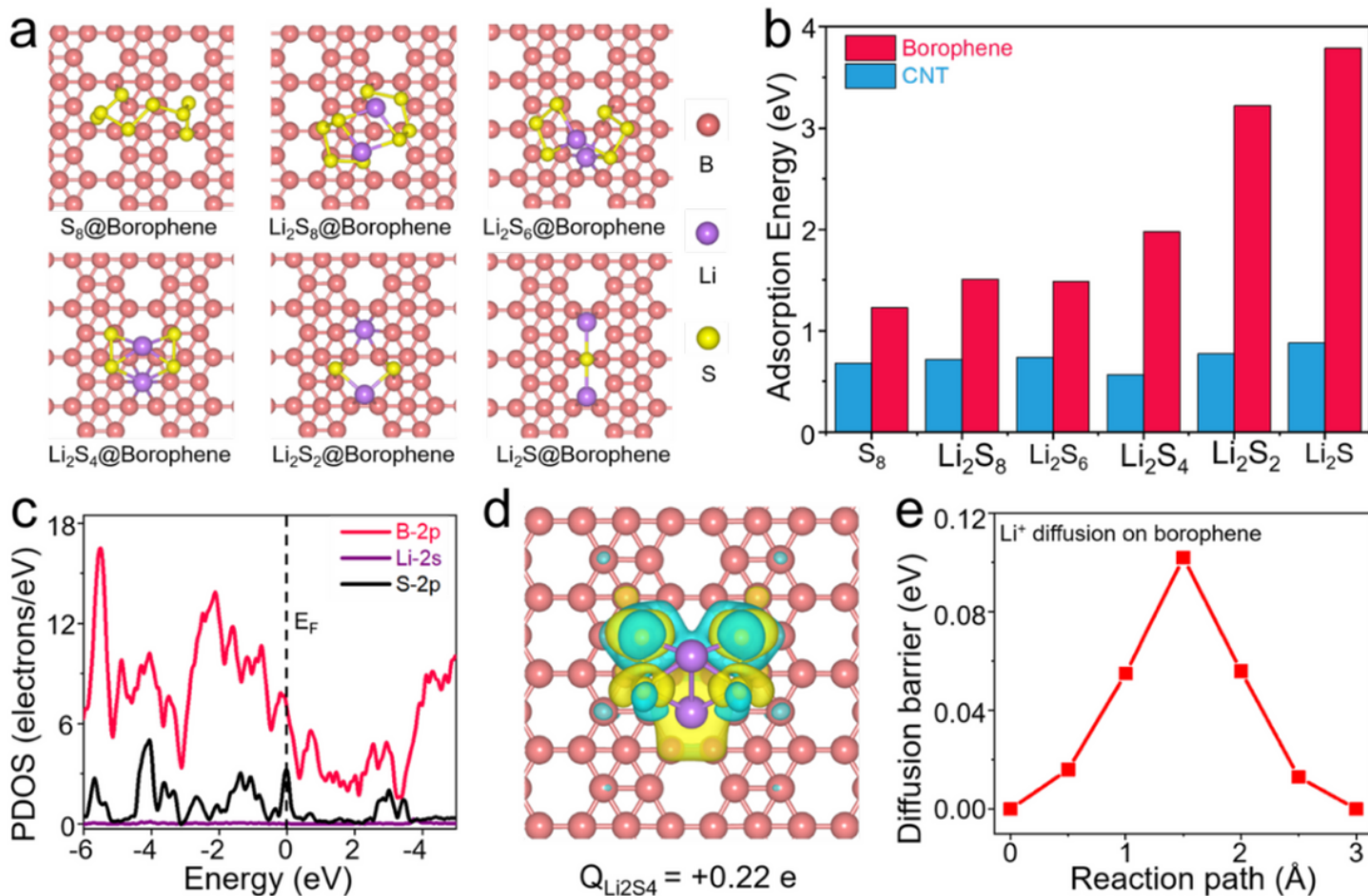


Figure 5

Theoretical study of the working mechanism of the CNT/B-based Li-S batteries. (a) Optimized adsorption configurations of S_8 and Li_2S_n ($n = 1, 2, 4, 6, 8$) on a monolayer $\beta 12$ -borophene. (b) Comparison of the adsorption energies of Li_2S_n on monolayer borophene and CNT. (c, d) Partial density of states (PDOS) and charge density difference of Li_2S_4 on borophene. The yellow and blue colors represent the spatial distribution with increased and decreased charge density, respectively. (e) Diffusion energy barrier of Li^+ on borophene.

Supplementary Files

This is a list of supplementary files associated with this preprint. Click to download.

- [SIBoropheneLiSbattery20210204.docx](#)